



24th COBEM - 2017



24th ABCM International Congress of Mechanical Engineering  
December 3-8, 2017, Curitiba, PR, Brazil

## COBEM-2017-1024

### TAILORING FLEXIBLE MICROCAPSULES FOR MOBILITY CONTROL

Débora F. do Nascimento

Jorge A. Avendaño

Ana Mehl

M. J. B. Moura

Marcio S. Carvalho

Pontifícia Universidade Católica do Rio de Janeiro, Rua Marquês de São Vicente, 225, Gávea, Rio de Janeiro/RJ - Brasil  
e-mail: [mnc@puc-rio.br](mailto:mnc@puc-rio.br)

**Abstract.** *Microcapsules are commonly used in the pharmaceutical, cosmetics, and food industries. Using a double emulsion microfluidic device, we are able to produce microcapsules with polymeric shells (cross-linkable PDMS). The mechanical properties of the microcapsules are controlled by both the thickness and polymer to cross-linker ratio of the polymeric shell. We obtain stress-strain curves for the microcapsules by squeezing the capsules between two parallel plates. We also perform experiments of flow of the microcapsules through a constricted capillary, measuring the pressure drop. The constricted microchannel serves as a model for a pore-throat geometry. Our final goal is to be able to produce microcapsules with specific mechanical properties and use them to control water mobility through heterogeneous porous media*

**Keywords:** *microcapsules, microfluidics, mobility control*

#### 1. INTRODUCTION

Soft microcapsule consists of a thin shell encapsulating a liquid core (Guo e Wyss, 2011; Kessler, Finken e Seifert, 2007). They are commonly used in the food, pharmaceutical, cosmetic and oil industries to encapsulate and release their contents (Chen, Brignoli e Studart, 2014; Fery e Weinkamer, 2007). In the application proposed here, they must retain their contents and maintain their mechanical resilience to selectively block pore throats to divert fluid flow in a porous medium (Duncanson *et al.*, 2015; Guillen *et al.*, 2012; Guillen, Carvalho e Alvarado, 2012). Emulsions and preformed polymer gels (PPG) enhance fluid flow resistance through confined spaces if their size is large relative to the characteristic geometries; in this way, they act as agents of mobility control. In addition, changes in the mechanical properties of the dispersed particles also affect the degree of mobility control. However, in emulsion and PPG systems, a single parameter defines their mechanical behavior, viscosity for emulsions and stiffness for PPGs; this severely limits their use as robust mobility control agents. A microcapsule with additional adjustable physical parameters including shell thickness and shell elastic modulus would have increased utility for a wide range of flow conditions and applications.

Highly controlled synthesis techniques such as droplet microfluidics could be used to prepare microcapsules with known and tunable mechanical properties; this enables control of size and membrane thickness through precise manipulation of fluid flow rates. In addition, microfluidics, particularly glass capillary microfluidics, affords the flexibility and choice of materials (Duncanson *et al.*, 2015) to impart various mechanical properties. An elastomer such as polydimethylsiloxane (PDMS) is an ideal shell material because it can sustain high elastic deformation (Fu *et al.*, 2014; Jiang *et al.*, 2012; Muñoz-Sánchez *et al.*, 2016; Vilanova, Rodríguez-Abreu, Fernández-Nieves, *et al.*, 2013). In addition, the mechanical properties (Johnston *et al.*, 2014; Wang, Volinsky e Gallant, 2014) of the shell can be tuned by changing the ratio of the two-component PDMS precursor (Jiang *et al.*, 2012). Despite the potential to tune the stiffness of PDMS microcapsules, this parameter remains unvaried for solid PDMS (Jiang *et al.*, 2012; Muñoz-Sánchez *et al.*, 2016; Zhao *et al.*, 2011), gas-filled (Agastin *et al.*, 2011; Duncanson *et al.*, 2015; Hettiarachchi e Lee, 2010) and liquid-filled microcapsules (Fu *et al.*, 2014; Vilanova, Rodríguez-Abreu, Fernández-Nieves, *et al.*, 2013).

To determine the overall microcapsule stiffness, single compression confinement methods (Chen, Brignoli e Studart, 2014; Duncanson *et al.*, 2015; Neubauer, Poehlmann e Fery, 2014; Rachik *et al.*, 2006; Vilanova, Rodríguez-Abreu, Fernández-Nieves, *et al.*, 2013) are commonly used. To determine the effect of the stiffness on their ability to reduce fluid mobility, the pressure drop associated with their blockage and passage through confined geometries was measured

(Cobos, Carvalho e Alvarado, 2009; Cui *et al.*, 2014; Duncanson *et al.*, 2015; Guillen *et al.*, 2012; Guillen, Carvalho e Alvarado, 2012; Li, Kumacheva e Ramachandran, 2013; Sun *et al.*, 2015). The combination of compression and constriction techniques provided a quantitative measurement of the elastic deformation of the microcapsules and their potential for use as mobility control agents in flow through porous materials. A well-characterized and elastically tunable PDMS shelled microcapsule could be used to adjust fluid mobility in complex porous media.

In this paper, we use microfluidics to prepare four different batches of PDMS-shelled microcapsules. Adjusting the fluid flow rates and the cross-link ratio of the two-component PDMS precursor we produce PDMS-shelled microcapsules with tunable elastic properties. We use single particle compression tests to measure their overall stiffness and flow them through constricted capillaries, thereby evaluating their potential to control fluid mobility.

## 2. EXPERIMENTAL METHODOLOGY

### 2.1. Fabrication of microcapsules with tunable elastic properties

A microfluidic glass capillary device was used to produce water-in-oil-in-water (W/O/W) double emulsions as templates for PDMS microcapsules. This device was fabricated in the laboratory with a microscope slide as a support; cylindrical and square glass capillaries; stainless steel needles as inlets; and the inlets were sealed with epoxy adhesive. The process started with a glass capillary that was heated and pulled simultaneously to a fine point employing an equipment named Micropipette puller<sup>®</sup> model P-1000. This capillary was placed within a square glass capillary. The outer diameter of the round capillary was approximately the same as the inner dimension of the square one, so a precise alignment was achieved and a coaxial geometry was formed. Also, both cylindrical and square capillaries were long enough to promote the precise alignment (Utada *et al.*, 2005, 2007).

Stainless steel dispensing needles with blunt tips and polypropylene luer lock hubs (inner diameter, ID, of 660.4 $\mu$ m and outer diameter, OD, of 914.4 $\mu$ m) were connected to non-sterile rigid but flexible micro medical grade polyethylene tubing (ID of 860 $\mu$ m and OD of 1.32mm). These tubing were connected to syringes containing the fluids of the inner, middle and outer phases. The fluids of inner and middle phases co-flow while the outer phase counter-flows. The flowing thread of fluid breaks up into a series of monodisperse droplets, due to the surface tension between the fluids (Fig. 1A). This configuration allows a low surface area, and hence, a low surface energy (Duncanson *et al.*, 2015; Utada *et al.*, 2005).

The microscopic images of procedure to obtain the four different polymer to cross-linker ratio systems (and their respective microcapsules): 5:1, 10:1, 17.5:1 and 20:1 are presented in Fig. 1B.

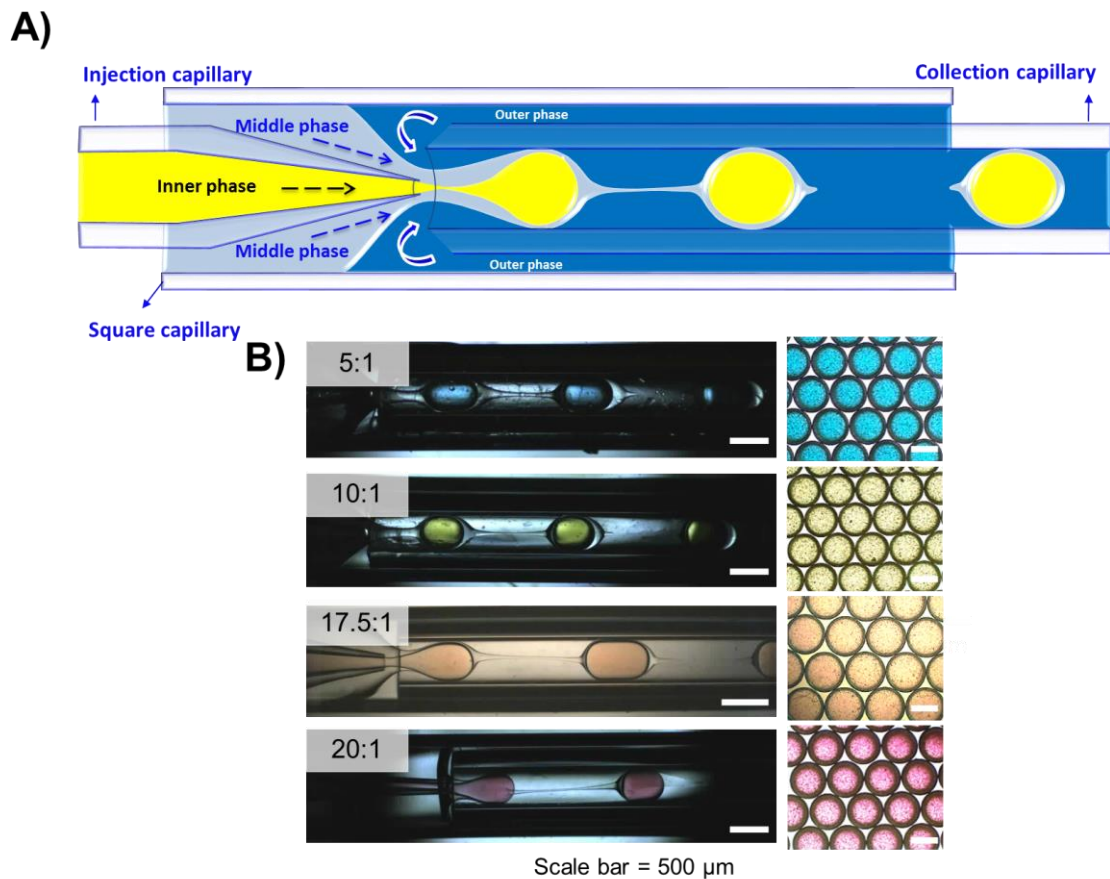


Figure 1. a) Schematic illustration of the microcapsules' production; b) microscopic view of the production for a single shell thickness from four different polymeric systems and their respective microcapsules

Three Harvard apparatus 11 Elite syringe pumps were used to control the flow rate of the three phases. A Leica DMi8 inverted microscope and a Photron Fast Camera were used to follow the procedure and adjust the flow rates. The inner phase was constituted by colored water (blue, yellow, orange or red). The colors were used to identify each polymer to crosslinker ratio and to facilitate in the characterization later on. The middle phase was constituted by the PDMS and the crosslinker (Sylgard 184<sup>®</sup> from Dow Corning base and curing agent), at four different ratios: 5:1, 10:1, 17.5:1 and 20:1 parts of polymer to parts of crosslinker. The outer phase was constituted by a water-based solution of poly(vinyl alcohol) (PVA) 10wt%. This polymer is used as a polymeric surfactant in microfluidic experiments as it provides interface stability as well as high shear stress due to its increased viscosity over diluted surfactant solutions (Duncanson *et al.*, 2015).

For each system, of specific polymer to crosslinker ratio, the flow rate of the middle phase was varied in order to assemble microcapsules with different shell thicknesses. At least five different flow rates of the middle phase were used for each system. The flow rates used to assemble the microcapsules are described in Table 1.

Table 1 – The flow rates used to assemble the four different systems

Capsules with polymer to crosslinker ratio:	Q inner (μL/h)	Q mid (μL/h)	Q outer (μL/h)
5:1	500	From 500 to 1500	2000
10:1	1500	From 200 to 1000	5000
17.5:1	2000	From 100 to 1700	5000
20:1	800	From 50 to 1200	4500

The 17.5:1 system is detailed in Fig. 2A, where it is possible to observe capsules obtained with six different shell thicknesses by increasing the ratio between the middle and inner fluids' flow rates. In Fig. 2B it is possible to observe the resultant mean outer diameter of the six different systems and their shell thicknesses over the radii with very precise control of the procedure. The tendency to increase the shell thicknesses over the radii was described in the literature and

it is compared to the data obtained. As it is possible to observe in Fig. 2B, our data is consistent with the predicted tendency. The shell thicknesses over the radii could be precisely tuned from 0.07 to 0.19 (Chen, Erb e Studart, 2012; Hennequin *et al.*, 2009; Vilanova, Rodríguez-Abreu, Fernández-Nieves, *et al.*, 2013).

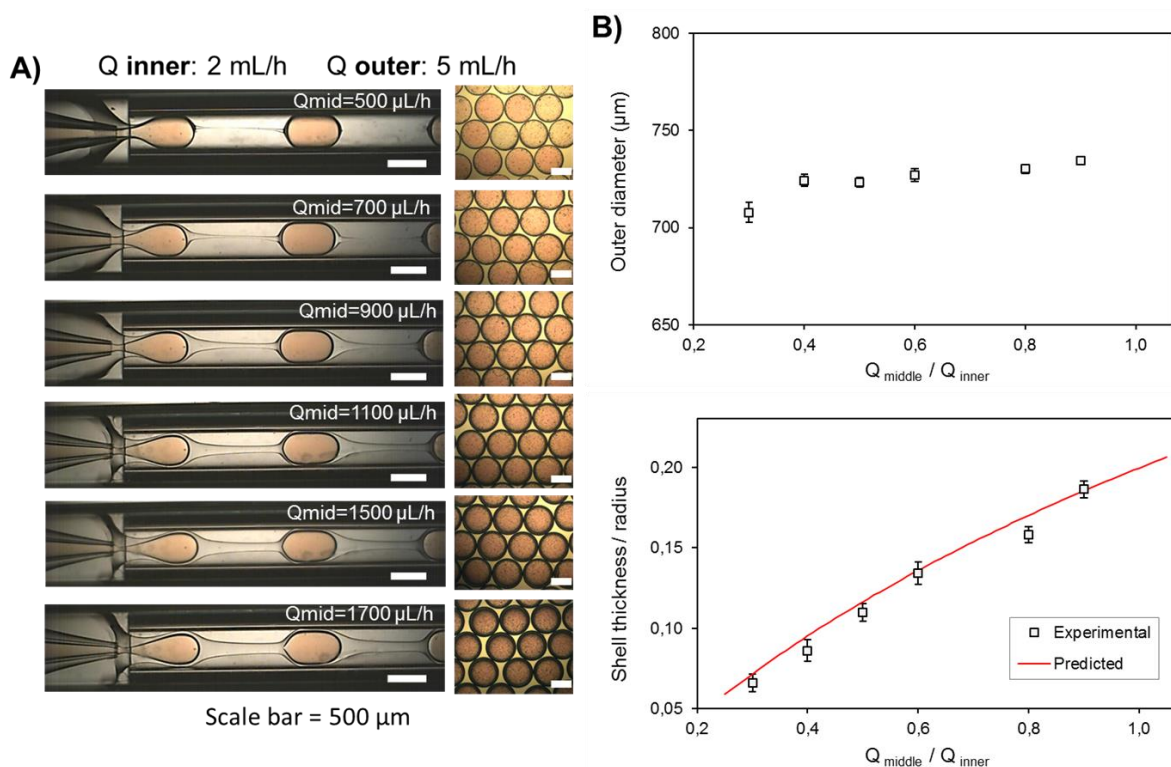


Figure 2. a) Microscopic view of the production of microcapsules with 17.5:1 polymer to crosslinker ratio with the indication of the flow rates used; b) Mean outer diameter and mean shell thicknesses over the radii as a function of the ratio between the middle and inner fluid flow rates

### 3. RESULTS

#### 3.1. Mechanical characterization of microcapsules

Our microfluidic technique combined with the use of PDMS elastomer enables us to precisely tune the mechanical properties of the microcapsules. To measure the mechanical properties and to evaluate the degree to which these parameters affect the overall stiffness, we conduct single particle compression tests. For each test, an individual microcapsule is submerged in water between two parallel plates on a rheometer.<sup>[24]</sup> Initially, the microcapsule is positioned between the two plates separated at a distance equivalent to the droplet diameter ( $2R$ ), as shown in Fig. 3a. As the top plate is incrementally lowered, the gap between the plates ( $2c$ ) decreases and the capsule deforms to an oblate spheroid-shape, as shown in Fig. 3b. At each position, the normal force ( $F$ ) is measured until the force reaches steady state.

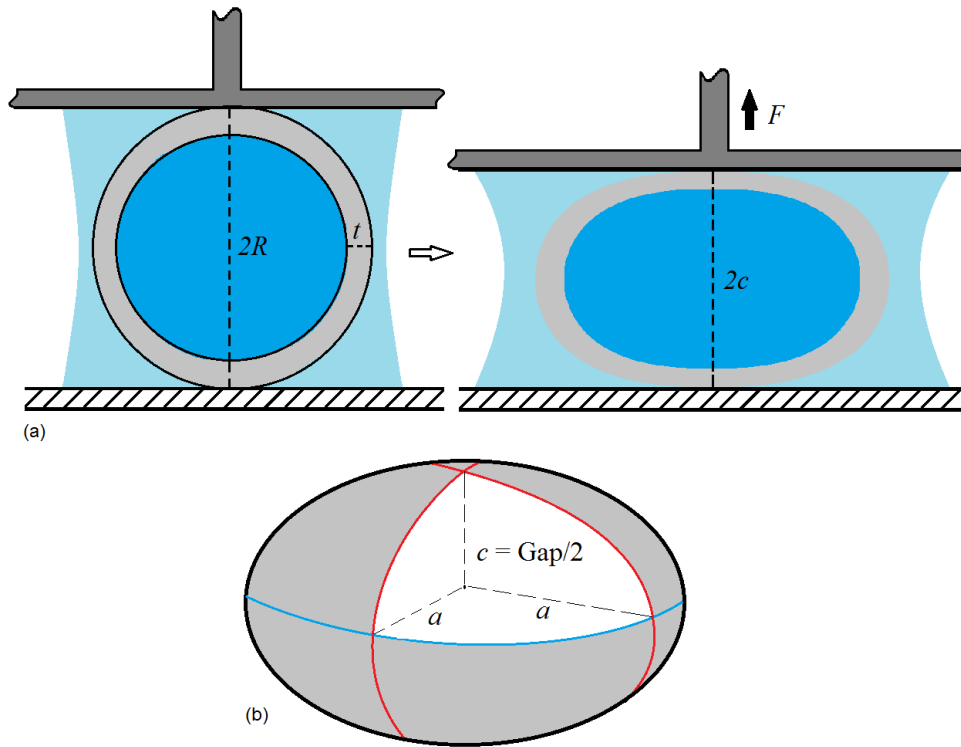


Figure 3. a) Sketch of compression test used to characterize the mechanical response of the produced microcapsules. b) Spherical capsules deform to oblate spheroids with radius  $a$ .

Assuming constant volume <sup>[25]</sup> of the compressed and uncompressed states the spheroid radius  $a$  is evaluated. The stress  $\sigma$  and the shell surface area  $A$  are evaluated at each plate position as shown in Equations 2 and 3:

$$\sigma = \left( \frac{F}{\pi a^2} \right); \quad (2)$$

$$A = 2\pi a^2 \left[ 1 + \left( \frac{1-c^2/a^2}{c/a} \right) \tanh^{-1}(c/a) \right]. \quad (3)$$

From these data, true area strain  $\varepsilon$  is calculated as shown in Equation 4, where the change in area  $\Delta A$  is the difference between  $A$  and  $A_0$ , the surface area of the uncompressed capsule.

$$\varepsilon = \ln \left( 1 + \frac{\Delta A}{A_0} \right). \quad (4)$$

We evaluate the apparent modulus as the ratio of the maximum stress to the maximum strain and plot these values as a function of thickness, as shown in Fig. 4.

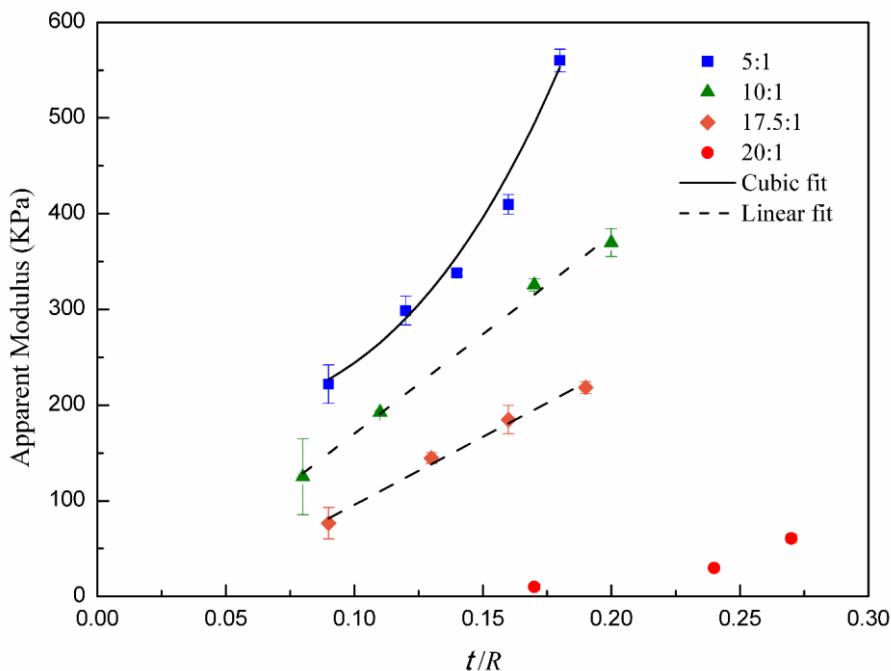


Figure 4. Apparent modulus, defined as the ratio of the maximum stress to maximum strain in the compression tests, as a function of shell thickness (in units of capsule radius) for the different polymer to cross-link ratio. The continuous line represents a cubic fit for the 5:1 results. Dashed lines represent a linear fit for the 10:1 and 17.5:1 systems.

Here, two trends are observed: one of a higher apparent modulus for higher cross-linked densities, and the other of a higher modulus for larger  $t/R$  values. In the former trend, a larger stress is required to deform the higher cross-linked density group (5:1), whereas the lowest stresses are required to deform the more flexible shells<sup>[19]</sup> due to use of the lower modulus bulk polymer<sup>[12]</sup>. This behavior is expected because the elastic modulus is inversely proportional to the cross-link density<sup>[19,26]</sup>. Furthermore, the second trend observed is that within each cross-linker density system, the overall microcapsule stiffness increases with  $t$ , thereby suggesting the shell thickness drastically influences the overall microcapsule stiffness.<sup>[17,18]</sup>

To further elucidate the effect of thickness within a given cross-linker ratio<sup>[5,17]</sup> we curve-fit the data, as shown in Fig. 4. The top curve representing the highest cross-linked density fits to a cubic power thus indicating the stress proportionality to the cubic thickness. This relationship shows the bending or flexural rigidity is the predominant contributor to the overall stiffness of the capsules prepared with the 5:1 PDMS. By contrast, the 10:1 and 17.5:1 curves are linear, hence emphasizing the importance of the stretching response for the lower cross-linked ratios. Unexpectedly, at the lowest cross-link ratio of 20:1, the shells become too fragile to withstand significant stress, consequently preventing evident data trends. The fragility of the shells with the lowest cross-linking ratio suggests there is a critical limit for which the cross-link ratio becomes more significant to the overall stiffness than does the shell thickness. Moreover, when shells are thin<sup>[2,25]</sup> bending is typically loosely defined and considered negligible. Consequently, the bending to stretching regime is solely defined as a thickness dependent condition. However, the differences between the curves in Fig. 4 for the various cross-linked densities indicate shell elasticity is also an important factor in the bending to stretching transition. A similar phenomenon is observed for thin blistering films<sup>[27]</sup> in which a dimensionless parameter,  $k$ , is proportional to the square root of the radius squared over the modulus. At a fixed thickness, increasing the Young's modulus lowers  $k$ . Consequently, the transition from bending to stretching is defined for low values of  $k$ , which corresponds to a higher stiffness. Regardless of the regime of deformation, all microcapsules will bend or stretch under stress; however, with the high cross-linked density, the stress is primarily attributed to bending, whereas for lower cross-linked density capsules, the stress is governed by stretching.

### 3.2. Flow of microcapsule suspensions through a constricted capillary

We hypothesize that the stiffer microcapsules will reduce fluid mobility to a larger extent than the softer microcapsules.<sup>[26]</sup> To evaluate this hypothesis, we flow the microcapsules through constrictions; these are prepared by using the capillary puller. A cylindrical glass capillary (with an inner diameter of 860  $\mu\text{m}$ ) is pulled to generate a constriction smaller than the average microcapsule diameter ( $2R = 707.5 \mu\text{m}$ ). The constriction diameter of approximately 400  $\mu\text{m}$  enables the microcapsules to deform to  $\sim 57\%$  of their initial diameter. By coupling a pressure transducer to the capillary flow system, the pressure changes caused by microcapsules restricting fluid flow can be monitored. For each

experiment, a syringe pump, set always at the same fixed volumetric flow rate, drives the microcapsule and its surrounding fluid (Milli-Q<sup>®</sup> water) through the constriction. The three positions (I, II, and III) of the microcapsule in the constriction are shown in Fig. 5a. These positions are directly correlated to the measured pressure difference ( $\Delta P$ ) as a function of time, shown in Fig. 5b. Each microcapsule position is defined by a distinct deformation regime: pre-deformation, maximum deformation, and recovery. The pre-deformation regime occurs when the microcapsule remains spherical prior to entering the constriction, as shown in Fig. 5a, I. In the pre-deformation regime, the position of the microcapsule is associated with the low-pressure region, shown in Fig. 5b, I; this pressure difference is equivalent to that of the suspending liquid alone. By contrast, a larger pressure is required to deform the capsule and push it through the capillary throat, as shown in Fig. 5b, II. As a result, in the maximum deformation state, the microcapsule deforms to a dumbbell shape thereby occupying the constriction and restricting fluid flow. The pressure increases to a maximum until the advancing microcapsule ceases to block fluid flow and it recovers to its initial spherical shape. The microcapsule then exits constriction into the wider opening of the unstricted region of the capillary; this transition is coupled to an immediate drop in pressure, seen in Fig. 5b, III.

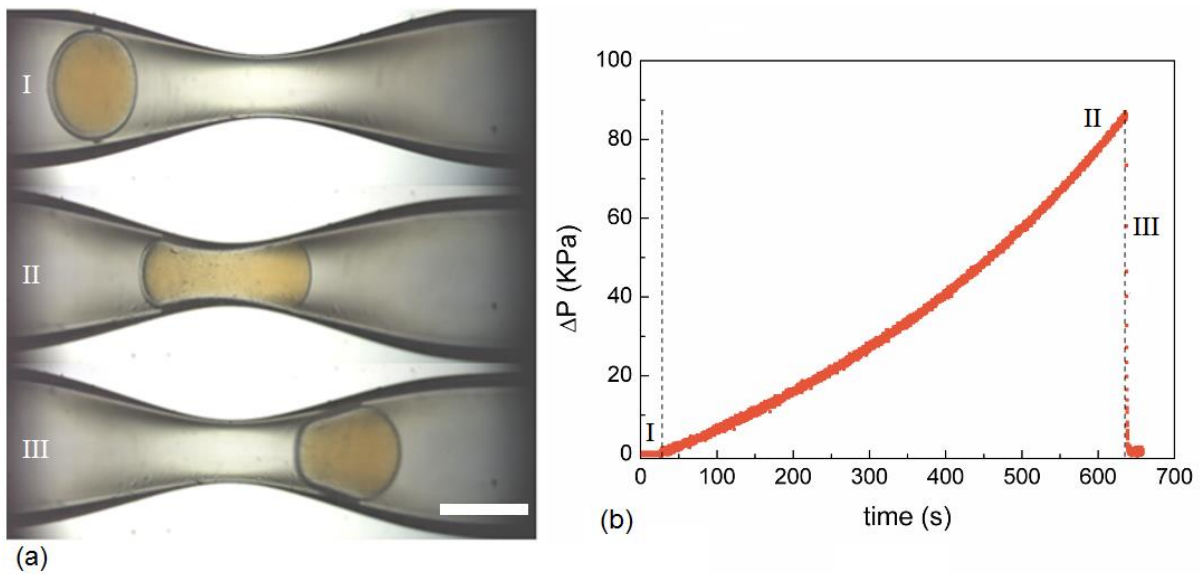


Figure 5. a) Images of microcapsule (17.5:1,  $t/R = 0.2$ ) deformation as it flows through the constriction. The scale bar is 500  $\mu\text{m}$ . b) Evolution of the pressure drop of the flow of a capsule and the suspending liquid through a constriction.

We plot the maximum pressure difference as a function of shell thickness  $t$  for each cross-link ratio to assess the impact of overall microcapsule stiffness on the ability of the microcapsule to change the mobility of the fluid flow, as shown in Fig. 6. As the thickness and stiffness increase, the resistance to fluid flow increases. For 5:1, the pressure increases with a slope of  $\sim 5$  and for the 20:1 increases with a slope of  $\sim 1$ .

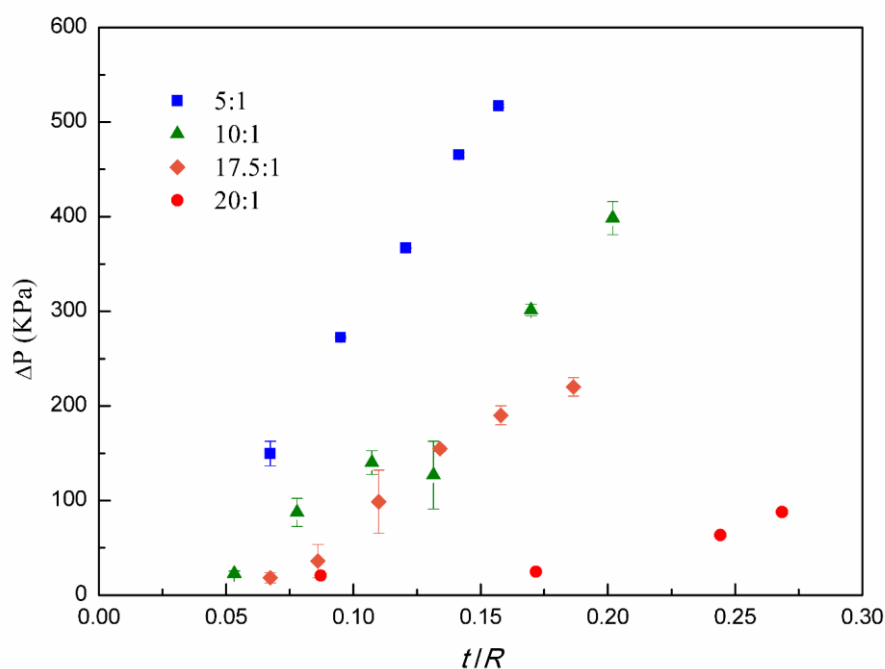


Figure 6. Maximum pressure drop of the flow through a constriction as a function of shell thickness and polymer to cross-link ratio. The mobility reduction associated with the capsule passing through the constriction is a function of both the bulk modulus of the polymer (polymer to cross-link ratio) and capsule shell thickness.

Moreover, the pressure for the 5:1 group is six times the highest pressure from the 20:1 group because the microcapsules with high overall stiffness (more rigid) require more pressure to deform.<sup>[20]</sup> In addition, there is a trend of increased pressure with shell thickness, which is somewhat disrupted by an outlier in the 10:1 group. Nevertheless, at the highest thickness values for each cross-linking ratio, the pressure is largest for the high cross-linking ratio (5:1), and smallest at the low ratio (20:1), signaling the proportionality between the overall microcapsule stiffness and the ability of the microcapsule to increase fluid flow resistance. Thus, the extent of mobility control can be tuned by the elastic properties of the microcapsules suspended in a continuous phase.

#### 4. FINAL REMARKS

Microcapsules with tunable elasticity were produced and studied with two different methods: 1) squeezing the capsules between two parallel plates, and 2) flowing the capsules through a constricted capillary and measuring the pressure drop. The results show that: a) the higher the polymer concentration the softer the capsule, and b) for the same polymer to cross-link ratio the thicker the capsule's shell the stiffer the capsule, both as expected. We also observed that the mobility reduction associated with the capsule passing through the constriction is a function of both the bulk modulus of the polymer (polymer to cross-link ratio) and the capsule's shell thickness.

The next step is to use the results of these studies to predict the mechanical properties of specific types of microcapsules. This would allow us to produce/select microcapsules according to their mechanical properties and use these capsules to control water mobility through heterogeneous porous media.

#### 5. ACKNOWLEDGEMENTS

This work was carried out in association with the ongoing Project registered as “Escoamento de dispersões complexas em meios porosos heterogêneos: análise na escala de poro e macrocópica” (PUC-Rio/Shell Brasil/ANP) – Complex Dispersion Flow Through Porous Media – funded by Shell Brasil under the ANP R&D levy as “Compromisso de Investimentos com Pesquisa e Desenvolvimento”.

## 6. REFERENCES

- AGASTIN, S. *et al.* Continuously perfused microbubble array for 3D tumor spheroid model. **Biomicrofluidics**, v. 5, n. 2, p. 24110, 2011.
- CHEN, P. W.; BRIGNOLI, J.; STUDART, A. R. Mechanics of thick-shell microcapsules made by microfluidics. **Polymer**, v. 55, n. 26, p. 6837–6843, 2014.
- CHEN, P. W.; ERB, R. M.; STUDART, A. R. Designer polymer-based microcapsules made using microfluidics. **Langmuir**, v. 28, n. 1, p. 144–152, 2012.
- COBOS, S.; CARVALHO, M. S.; ALVARADO, V. Flow of oil–water emulsions through a constricted capillary. **International Journal of Multiphase Flow**, v. 35, n. 6, p. 507–515, 2009.
- CUI, J. *et al.* Super-Soft Hydrogel Particles with Tunable Elasticity in a Microfluidic Blood Capillary Model. **Advanced Materials**, v. 26, n. 43, p. 7295–7299, 2014.
- DUNCANSON, W. J. *et al.* Microfluidic fabrication and micromechanics of permeable and impermeable elastomeric microbubbles. **Langmuir**, v. 31, p. 3489–3493, 2015.
- FERY, A.; WEINKAMER, R. Mechanical properties of micro- and nanocapsules: Single-capsule measurements. **Polymer**, v. 48, n. 25, p. 7221–7235, 2007.
- FU, Z. *et al.* Elastic silicone encapsulation of n-hexadecyl bromide by microfluidic approach as novel microencapsulated phase change materials. **Thermochimica Acta**, v. 590, p. 24–29, 2014.
- GUILLEN, V. R. *et al.* Capillary-driven mobility control in macro emulsion flow in porous media. **International Journal of multiphase flow**, v. 43, p. 62–65, 2012.
- GUILLEN, V. R.; CARVALHO, M. S.; ALVARADO, V. Pore Scale and Macroscopic Displacement Mechanisms in Emulsion Flooding. **Transport in Porous Media**, v. 94, n. 1, p. 197–206, 2012.
- GUO, M.; WYSS, H. M. Micromechanics of soft particles. **Macromolecular Materials and Engineering**, v. 296, n. 3–4, p. 223–229, 2011.
- HENNEQUIN, Y. *et al.* Synthesizing Microcapsules with Controlled Geometrical and Mechanical Properties with Microfluidic Double Emulsion Technology. **Langmuir**, v. 25, n. 14, p. 7857–7861, 2009.
- HETTIARACHCHI, K.; LEE, A. P. Polymer-lipid microbubbles for biosensing and the formation of porous structures. **Journal of Colloid and Interface Science**, v. 344, n. 2, p. 521–527, 2010.
- JIANG, K. *et al.* Microfluidic synthesis of monodisperse PDMS microbeads as discrete oxygen sensors. **Soft Matter**, v. 8, n. 4, p. 923–926, 2012.
- JOHNSTON, I. D. *et al.* Mechanical characterization of bulk Sylgard 184 for microfluidics and microengineering. **Journal of Micromechanics and Microengineering**, v. 24, n. 3, p. 35017, 2014.
- KESSLER, S.; FINKEN, R.; SEIFERT, U. Swinging and tumbling of elastic capsules in shear flow. **Journal of Fluid Mechanics**, v. 605, p. 20, 2007.
- LI, Y.; KUMACHEVA, E.; RAMACHANDRAN, A. The motion of a microgel in an axisymmetric constriction with a tapered entrance. **Soft Matter**, v. 9, n. 43, p. 10391, 2013.
- MUÑOZ-SÁNCHEZ, B. N. *et al.* Generation of micro-sized PDMS particles by a flow focusing technique for biomicrofluidics applications. **Biomicrofluidics**, v. 10, n. 1, p. 14122, 2016.
- NEUBAUER, M. P.; POEHLMANN, M.; FERY, A. Microcapsule mechanics: From stability to function. **Advances in Colloid and Interface Science**, v. 207, n. 1, p. 65–80, 2014.
- RACHIK, M. *et al.* Identification of the elastic properties of an artificial capsule membrane with the compression test: Effect of thickness. **Journal of Colloid and Interface Science**, v. 301, n. 1, p. 217–226, 2006.
- SUN, H. *et al.* Structure Governs the Deformability of Polymer Particles in a Microfluidic Blood Capillary Model. **ACS Macro Letters**, v. 4, n. 11, p. 1205–1209, 2015.
- UTADA, A. S. *et al.* Monodisperse Double Emulsions Generated from a Microcapillary Device. **Science**, v. 308, n. 5721, p. 537–541, 2005.
- \_\_\_\_\_. Dripping, Jetting, Drops, and Wetting: The Magic of Microfluidics. **MRS Bulletin**, v. 32, n. 9, p. 702–708, 2007.
- VILANOVA, N.; RODRÍGUEZ-ABREU, C.; FERNÁNDEZ-NIEVES, A.; *et al.* Fabrication of novel silicone capsules with tunable mechanical properties by microfluidic techniques. **ACS Applied Materials and Interfaces**, v. 5, n. 11, p. 5247–5252, 2013.
- \_\_\_\_\_. Fabrication of Novel Silicone Capsules with Tunable Mechanical Properties by Microfluidic Techniques. **American Chemical Society**, v. 5, p. 5247–5252, 2013.
- WANG, Z.; VOLINSKY, A. A.; GALLANT, N. D. Crosslinking effect on polydimethylsiloxane elastic modulus measured by custom-built compression instrument. **Journal of Applied Polymer Science**, v. 131, n. 22, 2014.
- ZHAO, L. B. *et al.* A novel method for generation of amphiphilic PDMS particles by selective modification. **Microfluidics and Nanofluidics**, v. 10, n. 2, p. 453–458, 2011.

## 7. RESPONSIBILITY NOTICE

The authors are the only responsible for the printed material included in this paper.